J Appl Electrochem (2014) 44:709–718
DOI 10.1007/s10800-014-0687-x

RESEARCH ARTICLE

Synthesis and electrochemical characterization on dual-doped $LiCoO_2$ via green chemistry method for lithium rechargeable batteries

R. Thirunakaran · Taewhan Kim · Won-sub Yoon

Received: 16 December 2013 / Accepted: 17 March 2014 / Published online: 6 April 2014

Abstract $LiCoO_2$ and $LiCu_xAl_yCo_{1-x-y}O_2$ ($x = 0.05$–0.15; $y = 0.05$–0.15) powders have been synthesized by sol–gel method using malic acid as chelating agent to obtain submicron sized particles. The synthesized samples have been subjected to spectral studies viz., differential thermal analysis (TG/DTA), fourier-transform infrared spectroscopy (FT-IR), X-ray diffraction (XRD), scanning electron microscopy (SEM), energy dispersive X-ray analysis (EDAX) and electrochemical characterization. XRD peak reflections of $LiCoO_2$ and $LiCu_xAl_yCo_{1-x-y}O_2$ exhibit high degree of crystallinity with better phase purity. SEM images of $LiCoO_2$ exhibit an ice cube surface morphology with grains size of 1.5 μm. Doped lithium cobalt oxide shows surface morphology of uniform particle size 2 μm. EDAX peaks confirm the actual composition of Cu, Al, Co and O in $LiCoO_2$ and $LiCu_xAl_yCo_{1-x-y}O_2$. Charge–discharge studies of undoped $LiCoO_2$ synthesized by sol–gel method deliver maximum an initial discharge capacity of 127 mA h g^{-1} which corresponds to columbic efficiency of 65 % during the first cycle with capacity fade of 0.13 mA h g^{-1} $cycle^{-1}$ over the investigated 10 cycles. Cu and Al doping $LiCoO_2$ exhibit the capacity fade of 0.06, 0.16, 0.14, 0.13 and 01.3 mA h g^{-1} $cycle^{-1}$ over the investigated 10 cycles corresponding to columbic efficiency of 74, 75, 73, 73 and 71 with capacity fade of 2, 3, 2, 2, and 2 mA h g^{-1} $cycle^{-1}$ at the 10th cycles for Cu: Al doping of 0.1:0.1, 0.13:0.07, 0.07:0.13, 0.15:0.05, and 0.05:0.15 respectively.

R. Thirunakaran (✉)
CSIR - Central Electrochemical Research Institute,
Karaikudi 630 006, Tamil Nadu, India
e-mail: rthirunakaran@gmail.com

T. Kim · W. Yoon
Department of Energy Science, Sungkyunkwan University,
Suwon-Si 440-746, Gyeonggi-do, Korea

Keywords Copper · Aluminium · Malic acid · Chelating agent · Sol–gel method · Layered lithium cobalt oxide · Spectral and electrochemical studies

1 Introduction

Layered $LiCoO_2$ is one of the most attractive candidates for rechargeable lithium batteries due to high voltage, good practical specific capacity (145 mA h g^{-1}), ease of preparation and an excellent cycle life [1–3], when compared with other layered oxide, and spinel and inverse spinel. $LiCoO_2$ is the most promising active cathode materials as it is widely employed in commercial lithium-ion batteries and it was the first reported to use as cathode material [4]. Albeit, the cost of $LiCoO_2$ is higher than spinel compound, several attempts have been made to improve the cell voltage and high specific capacity, by partially substituting di, tri, tetra and pentavalent metal cations via either by sol–gel method, combustion method or microwave method, thermal method [5–7]. Indeed, this material has an ordered rock salt structure (α-$NaFeO_2$ structure) and belongs to R3 m space group. Of late, many attempts are being taken to improve the electrochemical performance of $LiCoO_2$ either by doping/coating/dip-coating [8] or spin-coating [9–11] to achieve promising results for obtaining the higher specific capacity of stability of electrode than other layered and spinel compounds. This technique leads either to improve the capacity retention by suppressing the surface reactions of $LiCoO_2$ particles or higher achievable specific capacity by increasing the maximum intercalation voltage through the formation of stronger M–O bonds to stabilize the layered structure of $LiCoO_2$ with fully delithated state [12]. Now a days, thin films of $LiCoO_2$ are being prepared by plasma vacuum deposition method [13, 14]. Wet

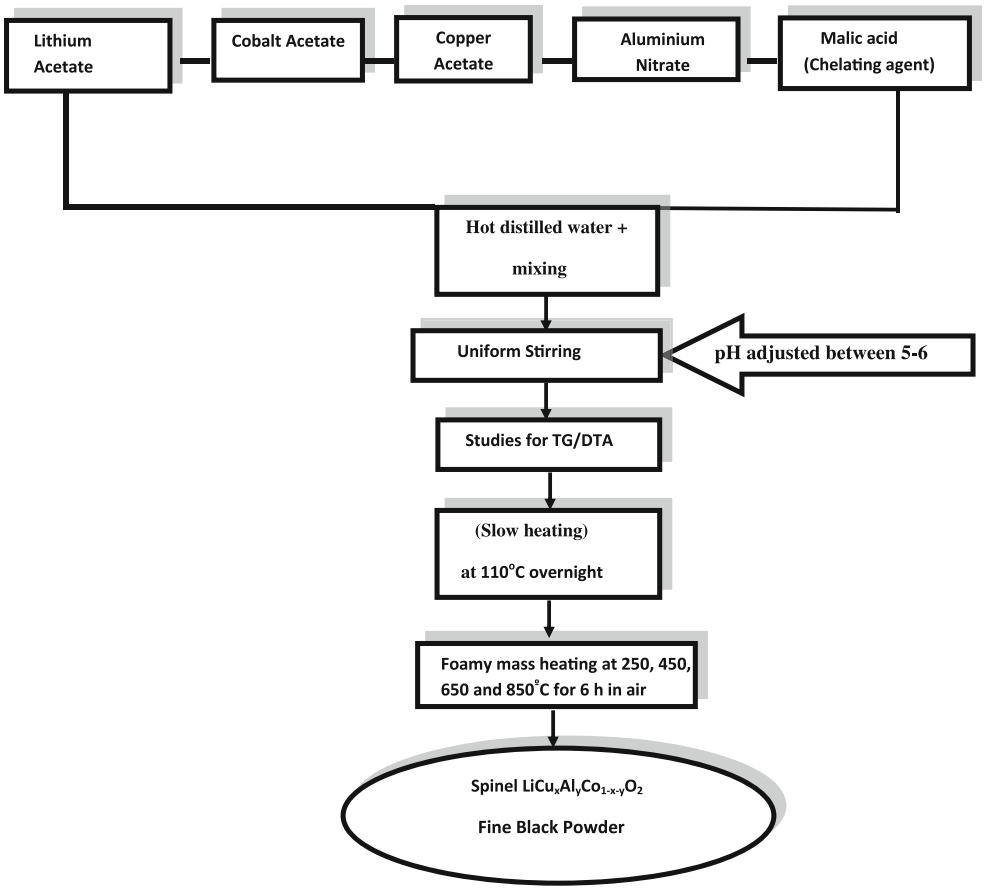

Fig. 1 Flow chart for synthesis of $LiCu_xAl_yCo_{1-x-y}O_2$ by sol–gel method using malic acid as chelating agent

chemistry like sol–gel method had been studied to synthesize and obtain the nano-sized particles to obtain good electrochemical stability of the compounds [15–17].

In this paper, an attempt has been made to stabilize the cobalt structure with ions like Cu^{2+}, Al^{3+} having equal or near equal ionic radius. It is interesting that the dopant ions Cu^{2+}, Al^{3+} combining stabilizes an ordered rock salt structure of ∞-$NaFe_2O_3$ and belongs to R3 m space group. We present multidoped-layered $LiCoO_2$ using malic acid as chelating agent via solution method and exhibiting an equal amounts of copper and aluminium ($LiCu_{0.10}Al_{0.10}Co_{0.80}O_2$) for better cycleability with good capacity retention owing to the low cation mixing leading to prevention of cationic disorder with good reversibility of the electrode reaction.

2 Experimental

Layered $LiCoO_2$ and $LiCu_xAl_yCo_{1-x-y}O_2$ ($x = 0.05$–0.15; $y = 0.05$–0.15) powders have been synthesized via sol-gel method using malic acid as chelating agent. Figure 1 depicts the flow chart of the synthesis procedure. Stoichiometric amounts of acetate of lithium, cobalt and the dopant salts such as copper acetate and aluminium nitrate were dissolved independently in triple-distilled water, and the ionic solutions were thoroughly mixed for obtaining homogeneity. Malic acid chelating agent has been added in the solution and stirred continuously with gentle heating till complete chelation takes place. The pH of the solution was maintained between 8 and 9, and the solution was slowly heated until a viscous gel is obtained. This gel mass was dried overnight in a hot air oven at 110 °C in order to obtain a dried mass. A small amount of the gel has been taken for TG/DTA analysis to understand the thermal behaviour and the rest of the gel mass is calcined at 850 °C for 6 h. For thermal analysis, the precursors are heated at a rate of 10 °C min^{-1} up to 850 °C in nitrogen atmosphere. All the calcined samples were subjected to physical studies such as TG/DTA, XRD, FTIR, SEM, EDAX and Galvano static charge–discharge cycling studies.

2.1 Coin cell Fabrication

Coin cells of 2016 configuration have been assembled in an argon-filled glove box (MBraun, Germany) using lithium

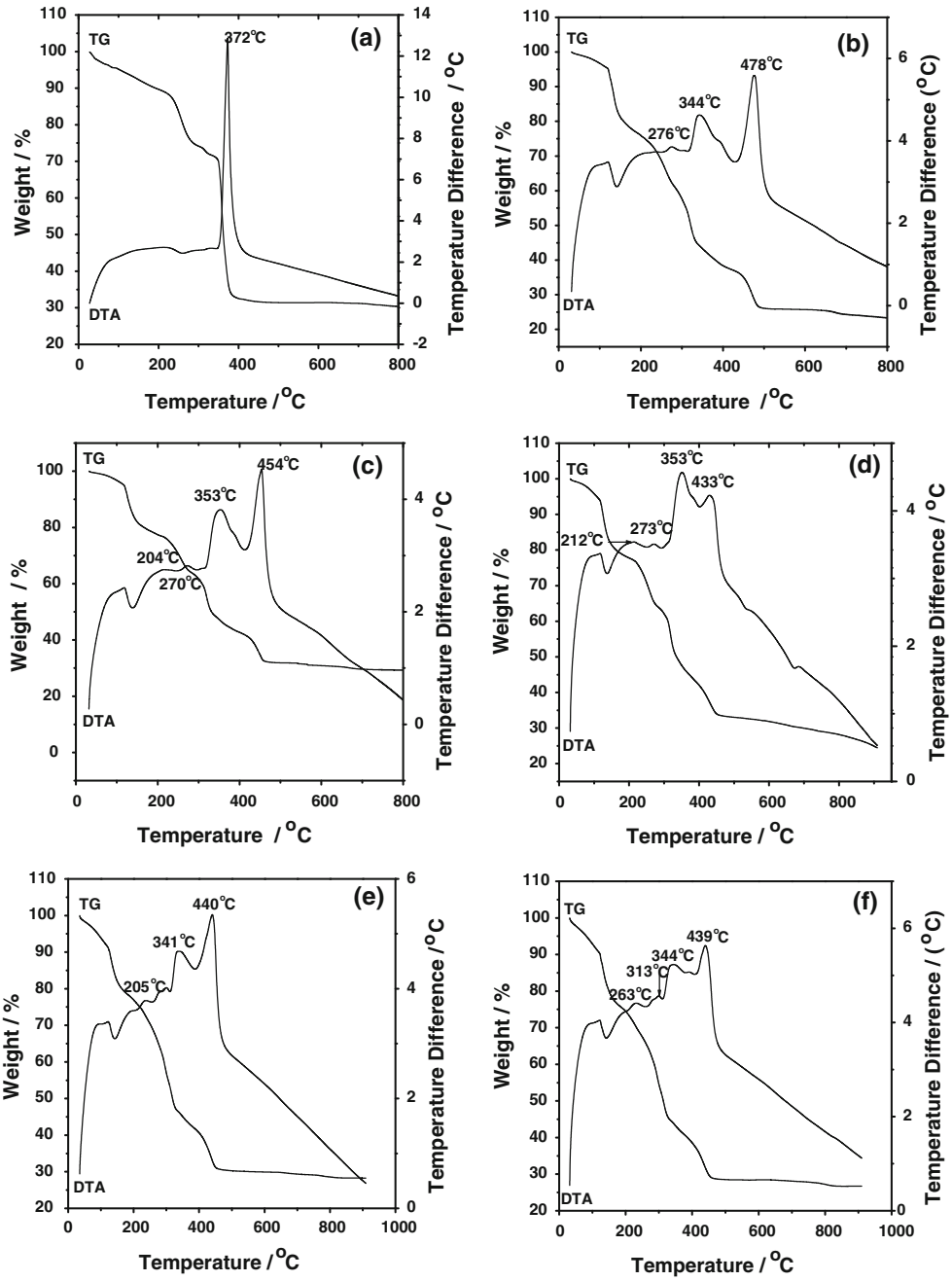

Fig. 2 Thermogravimetric and differential thermal analysis (TG/DTA) of $LiCoO_2$ and $LiCu_xAl_yCo_{1-x-y}O_2$ precursors. ($x = 0.05$–0.15; $y = 0.05$–0.15). **a** Undoped **b** Cu: 0.10; Al: 0.10; **c** Cu: 0.13; Al: 0.07; **d** Cu: 0.15; Al: 0.05; **e** Cu: 0.07 Al: 0.13; **f** Cu: 0.05; Al: 0.15

foil as anode, Celgard 2400 as separator, 1 M solution of $LiPF_6$ in 50:50 (v/v) mixture of ethylene carbonate (EC) and diethylene carbonate (DEC) as electrolyte and the synthesized material as cathode. The cathode is prepared by a slurry coating procedure from a mix comprising synthesized compound, carbon black and poly (vinylidene fluride) PVdF binder in *n*-methyl-2-pyrrolidone (NMP) solution mixed in the ratio 80:10:10 so as to form slurry. The slurry has been coated over aluminium foil and vacuum dried at 110 °C for 2 h. The dried coating has been pressed at an optimized pressure of 680 kg cm^{-1} for 2 min. Electrode blanks of 18-mm diameter are punched out and used as a cathode in the coin cell.

2.2 Electrochemical studies

The coin cells have been cycled at a constant current of C/10 rate between 2.8 and 4.2 V using an in-house battery cycling unit.

3 Results and discussion

3.1 Thermal studies

The TG/DTA curve of the $LiCoO_2$ precursor is depicted in Fig. 2a. The TG curve clearly shows three weight loss zones. At the beginning, the weight loss of 10 % up to 200 °C has been obtained which may be attributed to the removal of water. The next weight loss zone between 275 and 350 °C has been observed corresponding to major weight loss of 15 % and low weight loss 3 % owing to the decomposition of chelating agent (malic acid) and acetate and nitrate precursors. In the case of DTA curve, it shows a very sharp exothermic peak at 372 °C indicating the formation of layered and ordered $LiCoO_2$. Furthermore, TG curve clearly suggests that the thermal events completely cease above 400 °C.

The TG/DTA curves of (a) $LiCu_xAl_yCo_{1-x-y}O_2$ (b) Cu: 0.10; Al: 0.10, (c) Cu: 0.13; Al: 0.07, (d) Cu: 0.15; Al: 0.05, (e) Cu: 0.07; Al: 0.13, (f) Cu: 0.05; Al: 0.15 precursors synthesized via sol–gel route using malic acid as chelating agent are presented in Fig. 2b–f. For the $LiCu_{0.1}Al_{0.1}Co_{0.8}O_2$ sample, there are five weight loss zones. The first weight loss zone (10 %) has been observed up to 125 °C due to the removal of water molecules. The second and last fifth weight loss zone of 15, 35, 10 and 10 % have been obtained up to 500 °C which may also be assigned to the decomposition of the same nitrate and acetate precursors. As it can be seen in Fig. 2b, the DTA reflection shows one high intensity exothermic peak at 478 °C suggesting the formation of $LiCoO_2$ and two medium exothermic peaks at 344 and 276 °C. TG curve depicts the reaction stops beyond the 450 °C confirming the no further reaction takes place. It is quite interesting to note that among all dopant concentrations, $LiCu_{0.10}Al_{0.10}Co_{0.8}O_2$ sample shows the higher formation temperature (478 °C) than that of other all dopants which may be attributed as specific heat of Al (0.89 J/Kg K) is greater than Cu (0.38 J/kg K) and Co (0.42 J/Kg K) and usage of equal dopant ratio of (0.1 Cu; 0.1Al).

In the case of $LiCu_{0.13}Al_{0.07}Co_{0.8}O_2$ sample, TGA curve possesses the same five weight loss regions. DTA curve shows two well-defined exothermic peaks at 454 and 353 °C corroborating the formation of the compound with two small peaks at 204 and 207 °C. As far as thermal event of this compound is concerned, the reaction of TG has been stopped above 450 °C which is similar to that of $LiCu_{0.1}Al_{0.1}Co_{0.8}O_2$ sample.

For the $LiCu_{0.15}Al_{0.5}Co_{0.8}O_2$, $LiCu_{0.7}Al_{0.1}Co_{0.13}O_2$ and $LiCu_{0.05}Al_{0.15}Co_{0.8}O_2$ samples, five weight loss regions have been seen and well-defined two exothermic peaks (353, 433 °C); (341, 440 °C); (344, 439 °C) from each sample ratifying the formation of layered $LiCoO_2$ compound. Hence, all these three sample's precursors show the same similar thermal events above 500 °C stop without further reactions.

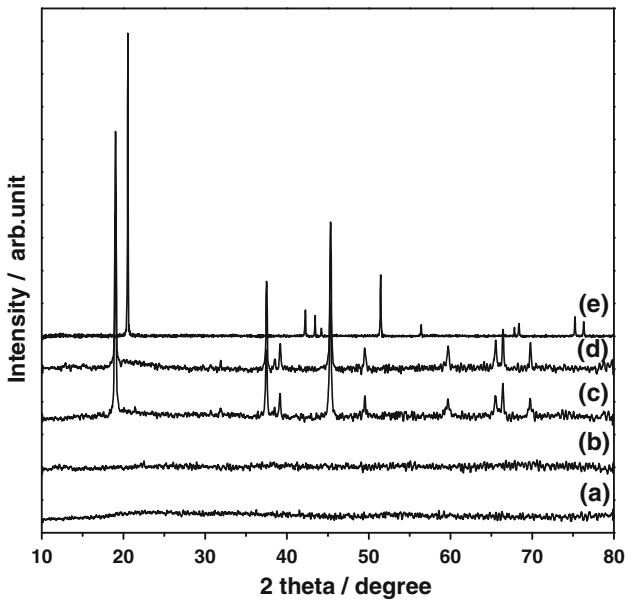

Fig. 3 XRD patterns of layered $LiCoO_2$ powders. **a** as synthesized, **b** 250 °C, **c** 450 °C, **d** 650 °C and **e** 850 °C

3.2 X-ray diffraction studies

Figure 3 depicts the XRD of layered $LiCoO_2$ samples calcined at different temperatures: (a) as synthesized, (b) 250 °C, (c) 450 °C, (d) 650 °C and (e) 850 °C. It is evident that as synthesized and the sample calcined at 250 °C show the hazy reflections suggesting that the materials are not suitable for electrochemical studies. In other words, the samples heated at 450 and 650 °C depict not ordered highly crystalline peaks and also indicate impurities peak such as Co_3O_4. The high intensity spectral reflections such as (003), (101), (006), (102), (104), (105), (009), (107), (108), (110) and (103) have been obtained for the sample calcined at 850 °C indicating that the synthesized compound is phase pure structure with highly crystalline peaks which are in good agreement with earlier researcher [18].

Figure 4 depicts the XRD patterns of $LiCoO_2$ samples calcined at 850 °C with different stoichiometric amounts of di and trivalent metal cations, viz., Cu and Al ($x = 0.05$–0.15; $y = 0.05$–0.15), synthesized via sol–gel method using malic acid as chelating agent. As it can be seen in Fig. 4a–f, all the diffraction peaks confirm to match perfectly with the Joint Committee and Powder Diffraction Standard (JCPDS card No. 16–0427). The spectral reflections of undoped and Cu–Al doped $LiCoO_2$ samples show

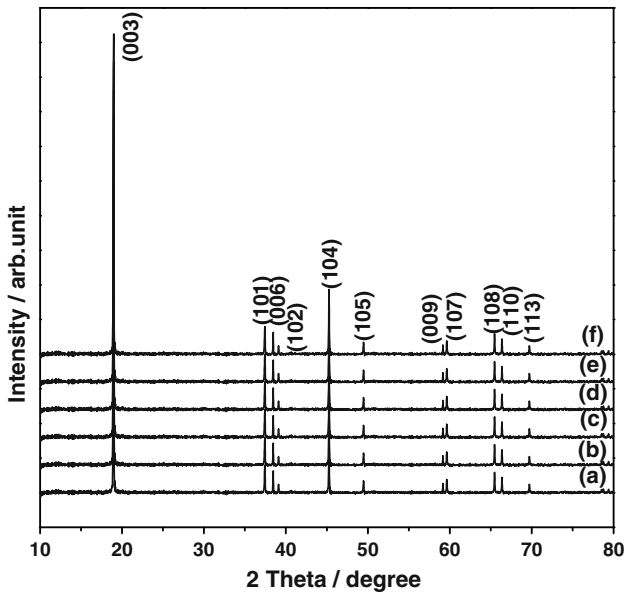

Fig. 4 XRD patterns of layered $LiCoO_2$ and Li $Cu_xAl_yCo_{1-x-y}O_2$ particles calcined at 850 °C: *a* undoped, *b* Cu: 0.10; Al: 0.10, *c* Cu: 0.13; Al: 0.07, *d* Cu: 0.15; Al: 0.05, *e* Cu: 0.07; Al: 0.13, *f* Cu: 0.05; Al: 0.15

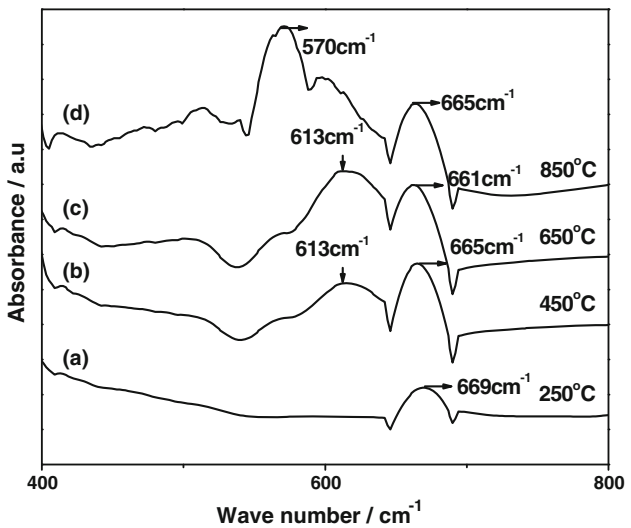

Fig. 5 FTIR spectra of $LiCoO_2$ particles calcined at different temperatures: *a* 250, *b* 450, *c* 650, *d* 850 °C

well-developed layered materials with better phase purity. Further, it is evident that all the peaks corresponding to (003), (101), (006), (102), (104), (105), (009), (107), (108), (110) and (103) which fall in line with other researchers [18–20]. The impurity peak (101) may be assigned resulting in the formation of Co_3O_4. All the peak signatures of undoped and doped compounds could be incorporated to α-$NaFeO_2$-layered structure with R3 m space group. In synthesizing the layered $LiCu_xAl_yCo_{1-x-y}O_2$, via sol–gel

Table 1 FTIR frequencies for peaks observed for $LiCoO_2$ calcined at different temperatures: (a) 250, (b) 450, (c) 650, (d) 850 °C

No.	Temperature (°C)	Wave number (cm^{-1})	Assignments
1	250	–	–
		669	Li–Co–O
2	450	613	Li–O
		665	Li–Co–O
3	650	613	Li–O
		665	Li–Co–O
4	850	570	Li–O
		665	Li–Co–O

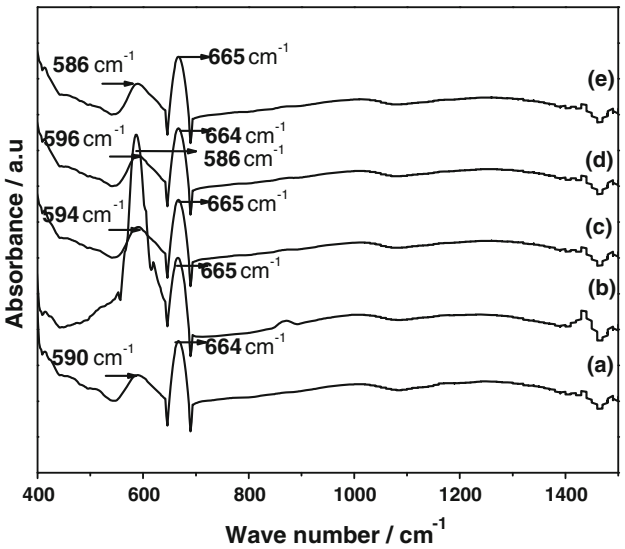

Fig. 6 FTIR spectra of Li $Cu_xAl_yCo_{1-x-y}O_2$ particles calcined at 850 °C. *a* Cu: 0.10; Al: 0.10, *b* Cu: 0.13; Al: 0.07, *c* Cu: 0.15; Al: 0.05, *d* Cu: 0.07; Al: 0.13, *e* Cu: 0.05; Al: 0.15

Table 2 FTIR frequencies for peaks observed for Li $Cu_xAl_yCo_{1-x-y}O_2$ calcined at 850 °C

No.	Sample	Wave number (cm^{-1})	Assignments
1	$LiCu_{0.1}Al_{0.1}Co_{0.8}O_2$	590	Li–O
		664	Li–Cu–Al–Co–O
2	$LiCu_{0.13}Al_{0.07}Co_{0.8}O_2$	596	Li–O
		665	Li–Cu–Al–Co–O
3	$LiCu_{0.15}Al_{0.5}Co_{0.8}O_2$	594	Li–O
		665	Li–Cu–Al–Co–O
4	$LiCu_{0.7}A_{l0.1}Co_{0.13}O_2$	596	Li–O
		664	Li–Cu–Al–Co–O
5	$LiCu_{0.05}A_{l0.15}Co_{0.8}O_2$	586	Li–O
		665	Li–Cu–Al–Co–O

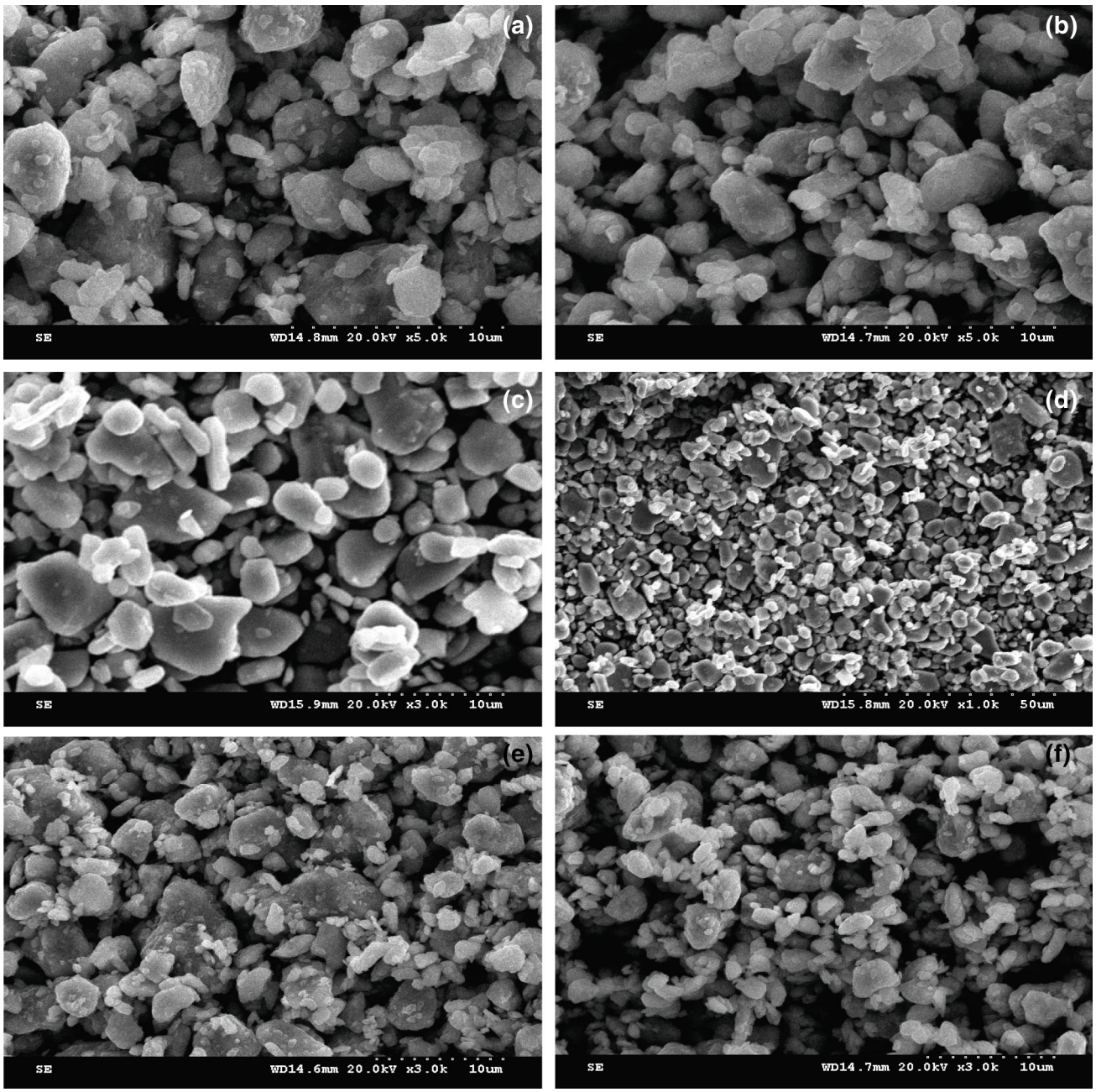

Fig. 7 SEM images of $LiCoO_2$ and $LiCu_xAl_yCo_{1-x-y}O_2$ calcined at 850 °C. **a** $LiCoO_2$; **b** $LiCu_{0.1}Al_{0.1}Co_{0.8}O_2$; **c** $LiCu_{0.13}Al_{0.07}Co_{0.8}O_2$; **d** $LiCu_{0.15}Al_{0.5}Co_{0.8}O_2$; **e** $LiCu_{0.7}Al_{0.1}Co_{0.13}O_2$; **f** $LiCu_{0.05}Al_{0.15}Co_{0.8}O_2$

method using malic acid as chelating agent, it facilitates the formation of metal ligand chain between Mn–O and COO^- resulting in the formation of highly crystalline phase pure layered materials.

3.3 FT-IR spectroscopy studies

The FT-IR spectra of the sol–gel derived $LiCoO_2$ particles calcined at different temperatures (250, 450, 650 and 850 °C) are depicted in Fig. 5. The spectra of the samples with low calcination temperature at 250 °C are seen around 669 cm^{-1} which may be attributed to the Co–O bending vibration mode. Also, another spectral band for Li–O disappears due to the low temperature. It is evident that the spectral reflections show similar behaviour for the stretching vibration of Co–O at wavelengths between 665 and 661 cm^{-1} for the sample calcined at 450 and 650 °C. Furthermore, the IR band for the samples calcined at high temperature (850 °C) has been shifted slightly towards a lower wave number (570 cm^{-1}) pertaining to Li–O. Table

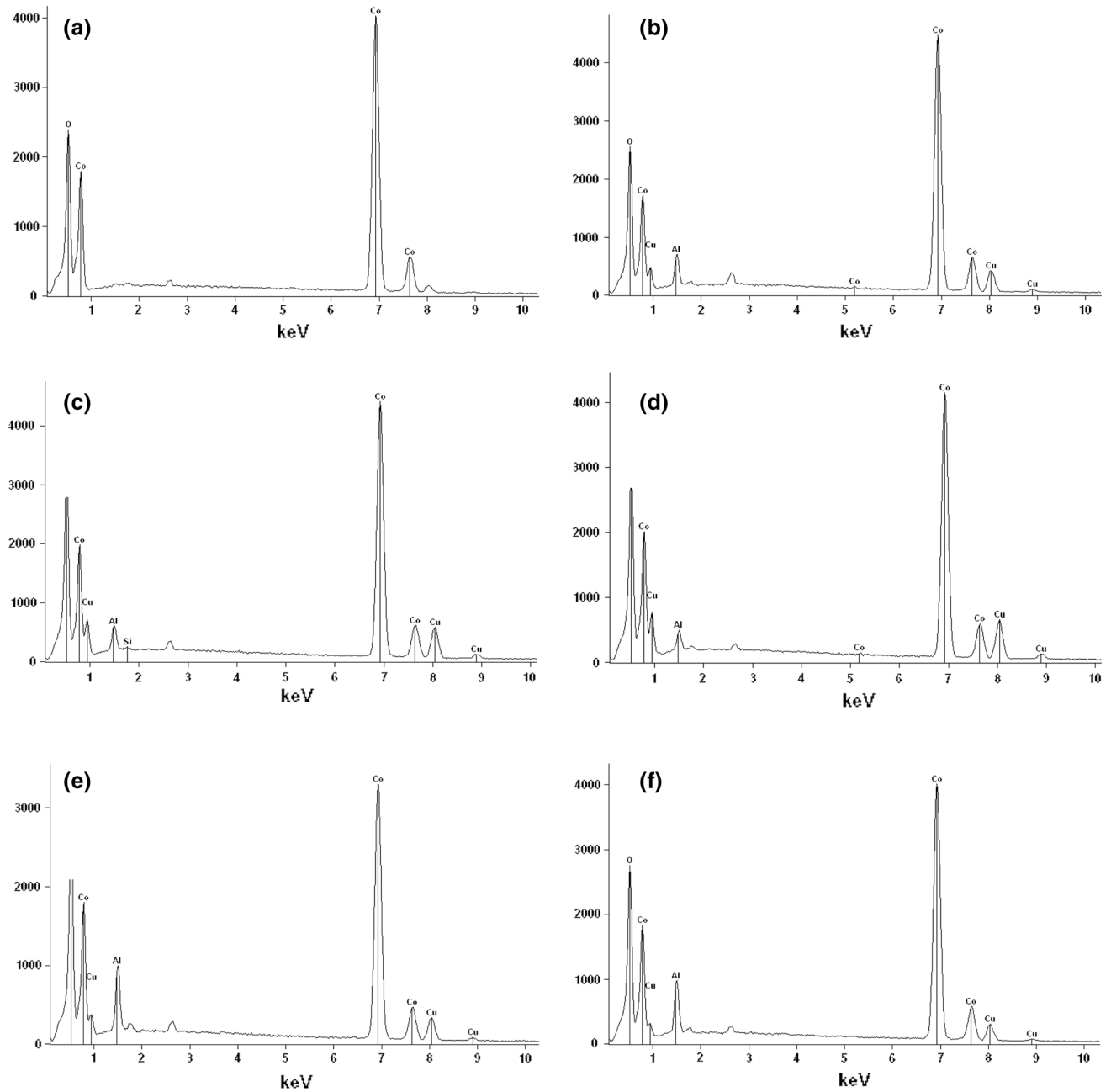

Fig. 8 EDAX profiles of $LiCoO_2$ and $LiCu_xAl_yCo_{1-x-y}O_2$ calcined at 850 °C. **a** $LiCoO_2$; **b** $LiCu_{0.1}Al_{0.1}Co_{0.8}O_2$; **c** $LiCu_{0.13}Al_{0.07}Co_{0.8}O_2$; **d** $LiCu_{0.15}Al_{0.5}Co_{0.8}O_2$; **e** $LiCu_{0.7}Al_{0.1}Co_{0.13}O_2$; **f** $LiCu_{0.05}Al_{0.15}Co_{0.8}O_2$

1 shows the FTIR frequencies for peaks observed for $LiCoO_2$ calcined at different temperatures.

Figure 6 illustrates FT-IR spectra of doped Li $Cu_xAl_yCo_{1-x-y}O_2$ particles. (a) Cu: 0.10; Al: 0.10, (b) Cu: 0.13; Al: 0.07, (c) Cu: 0.15; Al: 0.05, (d) Cu: 0.07; Al: 0.13, (e) Cu: 0.05; Al: 0.15. It is evident that the IR resonant frequencies of Li–O appear at lower wave number between 586 and 596 cm^{-1} and another spectral band at higher wave number between 586 and 665 cm^{-1} may be assigned to the Li–Al–Cu–Co–O stretching vibration band. Even if the dopant concentrations of Cu and Al increase variably, there is no much more shifting of peaks towards lower and higher wave numbers. Table 2 depicts the FTIR frequencies for peaks observed for Li $Cu_xAl_yCo_{1-x-y}O_2$ calcined at 850 °C.

3.4 SEM analyses

Figure 7 depicts SEM images of undoped $LiCoO_2$ and $LiCu_xAl_yCo_{1-x-y}O_2$. (a) $LiCoO_2$; (b) $LiCu_{0.1}Al_{0.1}Co_{0.8}O_2$;

Table 3 EDAX compositions of various elements in $LiCoO_2$ and $LiCu_xAl_yCo_{1-x-y}O_2$

No.	Element	Name of the compound	Weight %
1		$LiCoO_2$	
	O		57.45
	Mn		42.55
2		$LiCu_{0.1}Al_{0.1}Co_{0.8}O_2$	
	O		52.97
	Al		3.90
	Co		38.34
	Cu		4.78
3		$LiCu_{0.13}Al_{0.07}Co_{0.8}O_2$	
	O		58.21
	Al		2.69
	Co		33.03
	Cu		5.86
4		$LiCu_{0.15}Al_{0.5}Co_{0.8}O_2$	
	O		58.05
	Al		1.96
	Co		33.01
	Cu		6.98
5		$LiCu_{0.7}Al_{0.1}Co_{0.13}O_2$	
	O		60.13
	Al		5.83
	Co		30.26
	Cu		3.77
6		$LiCu_{0.05}Al_{0.15}Co_{0.8}O_2$	
	O		56.69
	Al		5.40
	Co		34.85
	Cu		3.05

(c) $LiCu_{0.13}Al_{0.07}Co_{0.8}O_2$; (d) $LiCu_{0.15}Al_{0.5}Co_{0.8}O_2$; (e) $LiCu_{0.7}Al_{0.1}Co_{0.13}O_2$; (f) $LiCu_{0.05}Al_{0.15}Co_{0.8}O_2$. The SEM picture of parent $LiCoO_2$ calcined at 850 °C (Fig. 7a) shows particle size of 1.5 μm with an ice cube surface morphology. It is evident that the particle size of all doped samples grows in size as dopant concentration is increased. $LiCu_{0.1}Al_{0.1}Co_{0.8}O_2$ and $LiCu_{0.13}Al_{0.07}Co_{0.8}O_2$ compounds illustrate the same size surface morphology with uniform particle size of 2 μm. At higher dopant of $LiCu_{0.15}Al_{0.5}Co_{0.8}O_2$ calcined at 850 °C, the particles in size have been observed higher with small agglomerated grains. Low doping of $LiCu_{0.7}Al_{0.1}Co_{0.13}O_2$, $LiCu_{0.05}Al_{0.15}Co_{0.8}O_2$ samples (Fig. 7e, f) depicts the same spherical grains with particle size of 1.5 and 1 μm, respectively. Doping equal ratio of Cu and Al ($LiCu_{0.1}Al_{0.1}Co_{0.8}O_2$) does not show any significant change of surface morphology and low particle size, while comparing to either low or high dopant ratio of the samples.

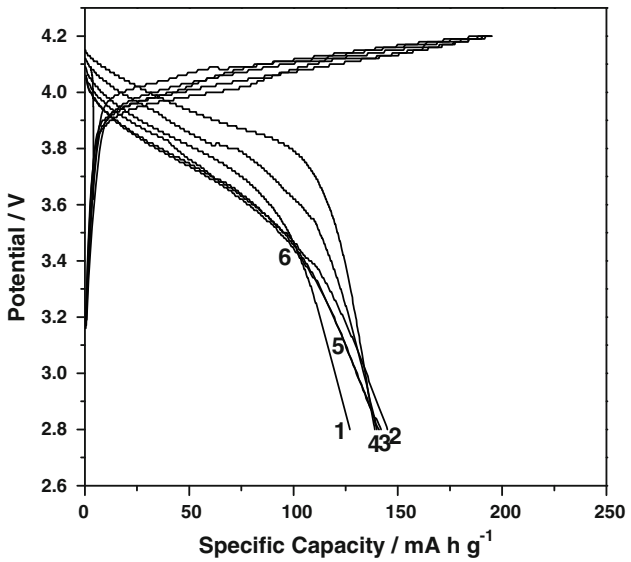

Fig. 9 First cycle charge–discharge behaviour of $LiCoO_2$ and $LiCu_xAl_yCo_{1-x-y}O_2$ calcined at 850 °C. *1* $LiCoO_2$; *2* $LiCu_{0.1}Al_{0.1}Co_{0.8}O_2$; *3* $LiCu_{0.13}Al_{0.07}Co_{0.8}O_2$; *4* $LiCu_{0.7}Al_{0.13}Co_{0.8}O_2$; *5* $LiCu_{0.15}Al_{0.5}Co_{0.8}O_2$ *6* $LiCu_{0.05}Al_{0.15}Co_{0.8}O_2$

3.5 EDAX analyses

Figure 8a–f depicts the EDAX profiles of $LiCoO_2$ and $LiCu_xAl_yCo_{1-x-y}O_2$. The spectral reflections of the above compounds suggest that the presence of elements and the compounds is pure. Table 3 shows the EDAX compositions of various elements in $LiCoO_2$ and $LiCu_xAl_yCo_{1-x-y}O_2$.

3.6 Galvanostatic charge–discharge studies

Electrochemical characterization studies have been carried out by galvanostatic charge–discharge cycling between 2.8 and 4.2 V at C/10 rate. Figure 9 (1–6) depicts the first cycle charge–discharge behaviour of $LiCoO_2$, and $LiCu_xAl_yCo_{1-x-y}O_2$ particles are calcined at 850 °C. Figure 9(1) depicts the undoped $LiCoO_2$ synthesized by sol–gel method delivers maximum an initial discharge capacity of 127 mA h g^{-1} against the charging capacity of 195 mA h g^{-1} which corresponds to columbic efficiency of 65 % during the first cycle with capacity fade of 0.13 mA h g^{-1} $cycle^{-1}$ over the investigated 10 cycles. It is quite interesting to note that the first cycle discharge capacity is as high as 127 mA h g^{-1} and at the 10th cycle is 110 mA h g^{-1} which is higher than that of other researchers synthesized bare $LiCoO_2$, via sol–gel method [21]. Nithya et al. [22] reported that undoped $LiCoO_2$ was synthesized via microwave synthesis method and delivered the maximum discharge capacity of 120 mA h g^{-1} during the first cycle which seems to be inferior in the present case. Cu and Al doping $LiCoO_2$ deliver discharge capacities of 145, 142, 141, 140 and 139 in Fig. 9.

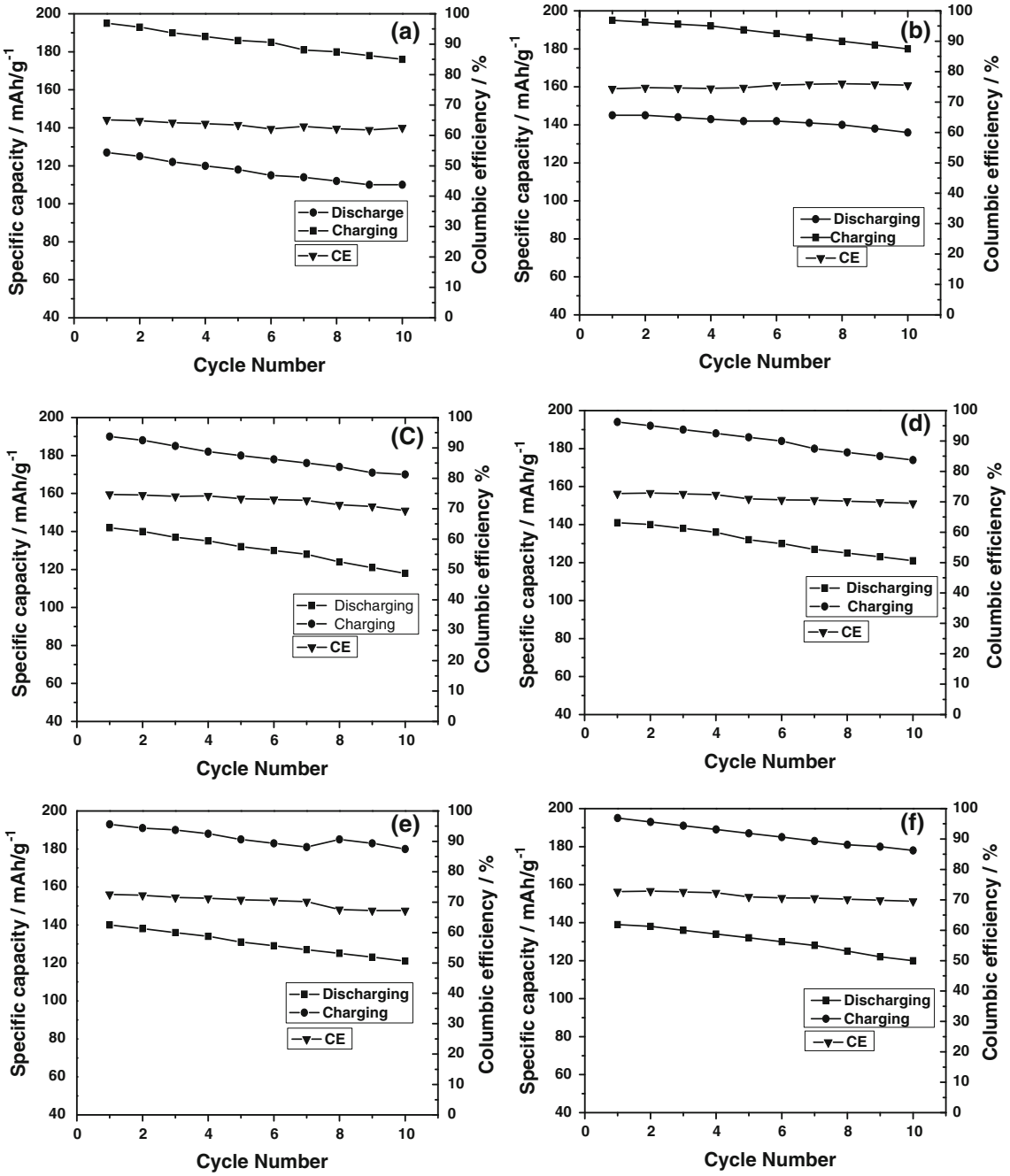

Fig. 10 Cycling behaviour of $LiCoO_2$ and $LiCu_xAl_yCo_{1-x-y}O_2$ calcined at 850 °C. **a** $LiCoO_2$; **b** $LiCu_{0.1}Al_{0.1}Co_{0.8}O_2$; **c** $LiCu_{0.13}Al_{0.07}Co_{0.8}O_2$; **d** $LiCu_{0.7}Al_{0.13}Co_{0.8}O_2$; **e** $LiCu_{0.15}Al_{0.5}Co_{0.8}O_2$; **f** $LiCu_{0.05}Al_{0.15}Co_{0.8}O_2$

(2–5) mA h g^{-1} during the first cycle corresponding to columbic efficiency of 74, 74, 72, 72 and 71, respectively.

Figure 10a–f depicts the cycling behaviour of $LiCoO_2$ and $LiCu_xAl_yCo_{1-x}O_2$ over the investigated 10 cycles with corresponding columbic efficiencies (CE).

Cycling performance of an equal amount of doping ration of Cu and Al using malic acid assisted $LiCu_{0.1}Al_{0.1}Co_{0.8}O_2$ (Fig. 10b) depicts maximum discharge capacity of 140 mA h g^{-1} corresponding to columbic efficiency of 72 % with capacity fade of 0.13 mA h g^{-1} cycle over the investigated 10 cycles and stabilizes the capacity retention at around 140 mA h g^{-1} when compared to all other dopants. At the end of 10th cycle, it delivers maximum stable discharge capacity of 136 mA h g^{-1} with capacity fade of 2 mA h g^{-1} $cycle^{-1}$.

In this paper, an attempt has been made to synthesize the layered oxide cathode materials using malic acid as chelating agent with di and trivalent cations to stabilize the

cobalt structure for improving the electrochemical stability of the compound.

Moreover, Cu and Al doping $LiCoO_2$ exhibits the capacity fade of 0.06, 0.16, 0.14, 0.13 and 01.3 mA h g^{-1} $cycle^{-1}$ over the investigated 10 cycles corresponding to columbic efficiency of 74, 75,73, 73 and 71 with capacity fade of 2, 3, 2, 2 and 2 mA h g^{-1} $cycle^{-1}$ at the 10th cycles for Cu and Al comprising to 0.1:0.1, 0.13:0.07, 0.07:0.13, 0.15:0.05 and 0.05:0.15, respectively.

Wang and coworkers [23] reported that $LiCu_{0.02}Co_{0.98}O_2$ synthesized via microwave-assisted sol–gel route and delivered an initial discharge capacity of 100 mA h g^{-1} during the first cycle, and at the 10th cycle the discharge capacity is around 90 mA h g^{-1} which is less than that reported by our present investigation.

Inter alia, all dopants, an equal amounts of copper and aluminium ($LiCu_{0.10}$ $Al_{0.10}Co_{0\cdot80}O_2$) stabilize the cobalt structure for better cycleability with good capacity retention owing to the low cation mixing leading to prevention of cationic disorder with good reversibility of the electrode reaction.

4 Conclusions

1. Layered $LiCoO_2$ and $LiCu_xAl_yCo_{1-x-y}O_2$ precursors (x = Cu-0.05–0.15; y = Al-0.05–0.15) have been synthesized via sol–gel method using malic acid as chelating agent to obtain micron-sized particles to use lithium rechargeable batteries.
2. SEM images of $LiCoO_2$ exhibit an ice cube surface morphology with grains size of 1.5 μm, while $LiCu_xAl_yCo_{1-x-y}O_2$ shows uniform particle size of 2 μm. EDAX peaks confirm the actual composition of Cu, Al, Co and O in $LiCoO_2$ and $LiCu_xAl_yCo_{1-x-y}O_2$.
3. Charge–discharge studies of $LiCoO_2$ deliver discharge capacity of 132 mA h g^{-1} corresponding to columbic efficiency of 95 % during the first cycle with capacity fade of 0.12 mA h g^{-1} $cycle^{-1}$ over the investigated 10 cycles. At the end of 10th cycles delivering maximum discharge capacity of 115 mA h g^{-1} with columbic efficiency of 93 % and capacity fade of 2 mA h g^{-1} $cycle^{-1}$.
4. $LiCu_{0.1}A_{l0.1}Co_{0.8}O_2$ delivers the discharge capacity of 140 mA h g^{-1} corresponding to columbic efficiency of 72 % with capacity fade of 0.13 mA h g^{-1} cycle over the investigated 10 cycles and stabilizes the capacity retention at around 140 mA h g^{-1}.
5. Therefore, it is concluded that an inter alia, all dopants, an equal amounts of copper and aluminium ($LiCu_{0.10}$ $Al_{0.10}Co_{0\cdot80}O_2$) stabilize the cobalt structure for better cycleability with good capacity retention owing to the low cation mixing leading to prevention of cationic disorder with good reversibility of the electrode reaction.

Acknowledgments The authors are grateful for the support given under 'Brain Pool program of the Korean Federation of Science and Technology Societies, Korea'.

References

1. Reimers JN, Dahn JR (1992) J Electrochem Soc 139(8):2091–2097
2. Garcia B, Farcy J, Pereira-Ramos JP, Baffier N (1997) J Electrochem Soc 144(4):1179–1184
3. Inaba M, Iriyama Y, Ogumi Z, Todzuka Y, Tasaka A (1997) J Ra-man Spectroscop 28(8):613–617
4. Misushima K, Jones PC, Wiseman PJ, Goodenough JB (1980) Mater Res Bull 15(6):783–789
5. Delmas C, Saadoune I, Rougier A (1993) J Power Sources 44:595–602
6. Lee KK, Kim KB (2000) J Electrochem Soc 147(5):1709–1717
7. Delmas C, Saadoune I (1992) Solid State Ion 53–56:370–375
8. Quinlan FT, Vidu R, Predoana L, Zaharescu M, Gartrner M, Groza J, Stroeve P (2004) Indus Eng Chem Res 43(10):2468–2477
9. Kim MK, Park YJ, Kim JG, Chung HT, Um WS, Kim MH, Kim HG J Power Source 99(1-2):34–40
10. Kim M, Chung HT, Park YJ, Kim JG, Son JT, Park KS, Kin HG (2002) Solid State Ionics 152–153:267–272
11. Rho YH, Kanamura K, Umegaki T (2003) J Electrochem Soc 150(1):A107–A111
12. Wang ZX, Chen LQ (2005) J Power Sources 146:254–258
13. Wei G, Haas TE, Goldner RB (1992) Solid State Ionics 58(1–2):115–122
14. Wang B, Bates JB, Hart FX, Sales BC, Zuhr RA, Robertson JD J Electrochem Soc 143(10)3203–3213
15. Sun YK, Oh IH, Hong SA (1996) J Mat Sci 3:3617–3621
16. Yoon WS, Kim KB (1999) J Power Sources 81–82:517–523
17. Song MY, Lee R (2002) J Power Sources 111(1):97–103 12
18. Zaheena CN, Nithya C, Thirunakaran R, Sivashanmugam A, Gopukumar S (2009) Electrochim Acta 54:2877–2882
19. Porthault H, Le Cras F, Franger S (2010) J Power Sources 195:6262–6267
20. Liao Li, Wang X, Luo X, Wang X, Gamboa S, Sebastian P (2006) J Power Sources 160:657–661
21. Fua LJ, Liua H, Lia C, Wua YP, Rahmb E, Holzeb R, Wua HQ (2005) Prog Mater Sci 50:881–928
22. Nithya C, Thirunakaran R, Sivashanmugam A, Gopukumar S (2011) J Power Sources 196:6788–6793
23. Prahasini P, Sivakumar M, Subadevi R, Wang FM (2012) Adv Mater Res 584:345–349